Vol. 50 (2019) *Acta Physica Polonica B* No 2

SHELL-MODEL DESCRIPTION IN ^{99}Rh AND SYSTEMATICS OF ODD-A Rh ISOTOPES

S. Kumar, S. Sihotra†, V. Singh, J. Rather, M. Kaur
J. Goswamy, N. Singh, D. Mehta

Department of Physics, Panjab University, Chandigarh-160014, India

T. Trivedi

Department of Pure and Applied Physics, Guru Ghasidas University
Bilaspur-495009, India

R.P. Singh, S. Muralithar

Inter-University Accelerator Centre, New Delhi-110067, India

R. Palit

Department of Nuclear and Atomic Physics, Tata Institute of Fundamental Research, Mumbai-400005, India

(Received November 14, 2018; accepted January 7, 2019)

Band structures of ^{99}Rh nucleus are discussed in framework of the spherical shell-model calculations using the $jj45pna$ effective interaction. Level structures at low energies are identified as resulting from the rotational bands based on the $\pi p_{1/2}$ and $\pi g_{9/2}$ configurations. The lowest observed positive-parity state is $9/2^+$ and corresponds to wave function consisting of the $\pi(p^2_{1/2}g^5_{9/2}) \otimes \nu(g^2_{7/2}d^2_{5/2})$ configuration. Systematics of single-quasiparticle $\pi p_{1/2}$ and $\pi g_{9/2}$ bands in odd-A $^{91-113}$Rh isotopes along with the ground state bands in the corresponding even–even Ru core isotopes is discussed to bring out the role of spin–orbit partner orbitals for collectivity. The energy staggering plots for odd-A $^{91-113}$Rh isotopes are also discussed.

DOI:10.5506/APhysPolB.50.159

† Corresponding author: `ssihotra@pu.ac.in`

1. Introduction

Nuclei with neutron number in vicinity of the major shell closure at $N = 50$, and the proton number lying between the semi-closed $Z = 40$ and the closed $Z = 50$ shells provide particularly good platform to probe the weakly deformed nuclei. Theoretical interpretations of level structures from new spectroscopic studies in these nuclei have revealed novel deformation-generating mechanisms [1–4]. In this mass region, the coexistence of spherical and deformed shapes results in complex level structure. The proton–neutron ($\pi\nu$) residual interaction predominates in odd–odd nuclei. The role of proton–neutron interaction and/or core excitation in the shell-model structure of $N = Z$ nuclei gained impetus in recent studies. The Rh ($Z = 45$) isotopes with the proton Fermi surface in the middle of the $g_{9/2}$ proton shell (half-particle and half-hole) provide a platform for various intriguing phenomena. Structure of these nuclei is affected by change in the neutron number, especially the neutron valence space with reference to the $N = 50$ core consisting of the $\nu d_{5/2}$, $\nu g_{7/2}$, $\nu d_{3/2}$ and $\nu s_{1/2}$ orbitals. The prolate-driving low-Ω $\nu h_{11/2}$ intruder orbital starts filling up in the case of the Rh isotopes with neutron number above $N \approx 54$, and the configuration-dependent triaxiality is achieved due to the competing shape-driving ability of the $\nu h_{11/2}$ and $\pi g_{9/2}$ orbitals [5–7]. The odd-A and odd–odd Rh isotopes involving the $\pi g_{9/2} \otimes \nu h_{11/2}$ and $\pi g_{9/2} \otimes (\nu h_{11/2})^2$ configurations, respectively, exhibit minima in the potential-energy surfaces for the triaxial nuclear shape with large positive γ parameter, and signatures of triaxiality have been observed in these bands. In the case of the lighter isotopes, the $\nu h_{11/2}$ orbitals are accessible at increasing excitation energies. The other neutron and proton states originating from the normal-parity subshells are not drive deformation driving, except the intruder $[431]1/2^+$ proton orbital originating from the $\pi g_{7/2}$ subshells located above $Z = 50$ major shell gap. Further, large spatial overlap between the $\nu g_{7/2}$ and $\pi g_{9/2}$ spin–orbit partner (SOP) orbitals accentuates the importance of strong $\pi\nu$ interaction. Three quasiparticle configurations containing these orbitals are expected to compete with other three quasiparticle configurations involving aligned $\nu h_{11/2}$ neutron pair [8, 9]. In the present work, shell-model calculation has been performed for the recent observed band structures [10]. In the calculations, the model space involves protons in the $2p_{1/2}$ and $g_{9/2}$ orbitals, and neutrons in the $2d_{5/2}$, $3s_{1/2}$, $2d_{3/2}$, $1g_{7/2}$ and $1h_{11/2}$ orbitals. A systematic comparison of single-quasiparticle $\pi g_{9/2}$ and $\pi p_{1/2}$ bands in the odd-A Rh isotopes is presented in the paper. The systematic of odd-A Rh isotopes for the importance of spin–orbit partner orbitals for deformation in this region is also discussed.

2. Spherical shell-model description

Theoretical shell-model calculations using different model spaces as different two-body interactions have been successful in reasonable understanding of the observed level structure at low and medium spins for nuclei in the $A = 100$ mass region [11–13]. These calculations are also quite feasible in ^{99}Rh nucleus as there are not too many active particles. The shell-model calculations provide a microscopic basis for the collective types of approach. In order to interpret the recently observed level structure of ^{99}Rh (Fig. 1), state-

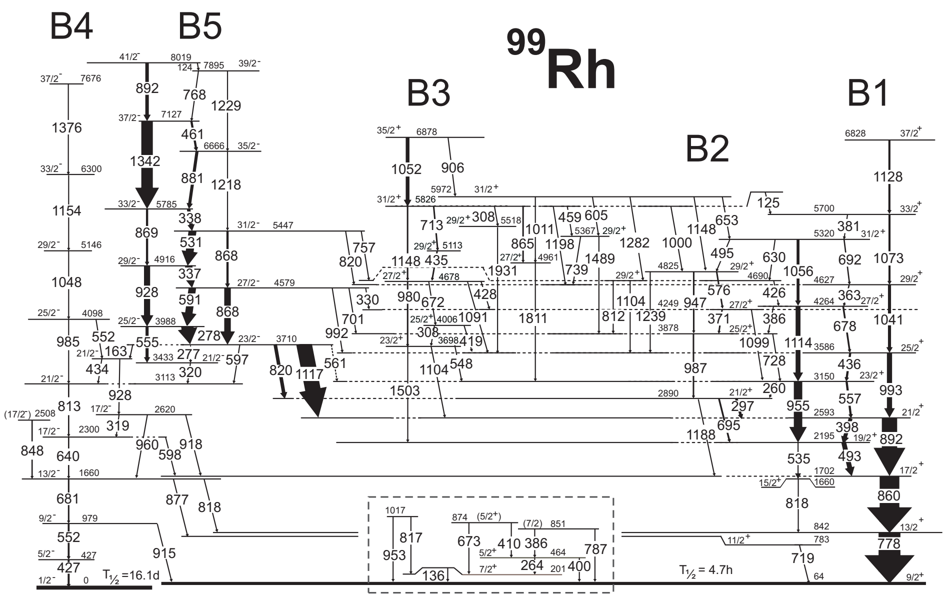

Fig. 1. Shell-model calculations are performed for the shown levels scheme of ^{99}Rh, which is presented in recent work [10]. Inset shows low spin part from the decay of ^{99}Pd [14]. Energies of γ rays and levels are given in keV. The width of the arrows is proportional to the relative γ-ray intensity. Identified band structures are labeled B1–B5.

of-the-art shell-model calculations have been performed using NuShell [15] computer code. The calculations have been carried out by taking $^{78}_{38}$Sr as core and $jj45pn$ model space involving valence protons distributed over the single-particle $2p_{1/2}$ and $1g_{9/2}$ orbitals and neutrons occupying $1g_{7/2}$, $2d_{5/2}$, $2d_{3/2}$ and $3s_{1/2}$ orbitals with maximum four particles allowed in $d_{5/2}$ orbital. The $jj45pna$ effective interaction has been used in the calculations and the corresponding two-body matrix elements were obtained from the work of Hjorth–Jensen [16]. A comparison of the experimental excitation energies of the positive and negative-parity states of ^{99}Rh with the corresponding theoretical spectra is shown in Fig. 2. As the $h_{11/2}$ orbital is not included in the calculations, the positive-parity states in bands B1 and B2, and the negative-parity states in band B4 have been included for comparison with the predicted ones. The details of the wave functions for the excited higher spins states of positive- and negative-parity states of ^{99}Rh corresponding to the experimental ones are given in Table I.

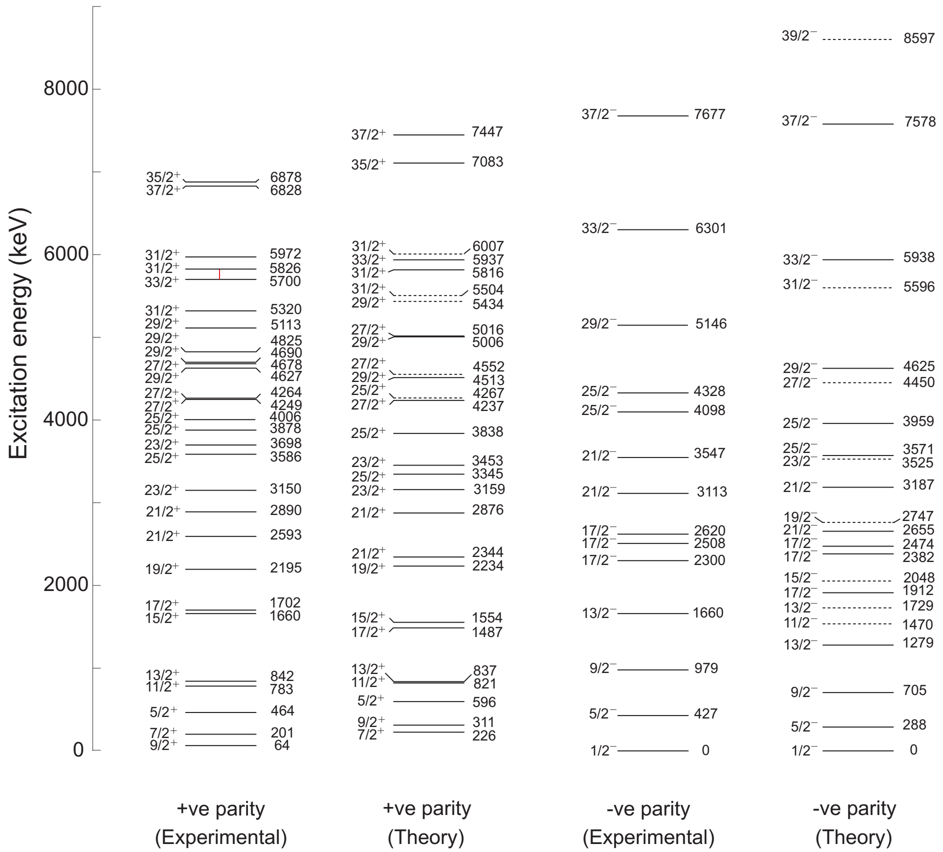

Fig. 2. Comparison of the excitation energies of various experimentally observed states in ^{99}Rh with those calculated using shell model [15].

It is evident from Fig. 2 that the shell-model calculations exhibit good agreement with the experimental level energies for positive-parity states. The shell-model calculations reproduce the low-lying $7/2^+$, $11/2^+$ and $13/2^+$ states very well with an energy difference of 25, 38 and 5 keV, respectively, whereas the other calculated excitation energies for the levels with spin $I = 17/2^+$, $19/2^+$, $21/2^+$, $23/2^+$, $25/2^+$, $27/2^+$, $29/2^+$ and $31/2^+$ of positive parity bands have reasonable good agreement with the experimental results. The calculations predict the $9/2^+$ state to be 85 keV above the $7/2^+$ state,

TABLE I

Wave functions for protons and neutrons in ^{99}Rh for the ground state and the excited states in bands B1, B2 and B4.

Spin	Probability	Wave function for protons	Wave function for neutrons	Spin	Probability	Wave function for protons	Wave function for neutrons
$7/2^+_1$	31%	$p^2_{1/2}g^5_{9/2}$	$g^2_{7/2}d^2_{5/2}d^0_{3/2}$	$35/2^+_1$	38%	$p^2_{1/2}g^5_{9/2}$	$g^1_{7/2}d^2_{5/2}d^1_{3/2}$
$9/2^+_1$	30%	$p^2_{1/2}g^5_{9/2}$	$g^2_{7/2}d^2_{5/2}d^0_{3/2}$	$37/2^+_1$	35%	$p^2_{1/2}g^5_{9/2}$	$g^1_{7/2}d^3_{5/2}d^0_{3/2}$
$5/2^+_2$	27%	$p^2_{1/2}g^5_{9/2}$	$g^2_{7/2}d^2_{5/2}d^0_{3/2}$	$1/2^-_1$	35%	$p^1_{1/2}g^6_{9/2}$	$g^2_{7/2}d^2_{5/2}d^0_{3/2}$
$11/2^+_1$	21%	$p^2_{1/2}g^5_{9/2}$	$g^2_{7/2}d^2_{5/2}d^0_{3/2}$	$5/2^-_1$	30%	$p^1_{1/2}g^6_{9/2}$	$g^2_{7/2}d^2_{5/2}d^0_{3/2}$
$13/2^+_1$	28%	$p^2_{1/2}g^5_{9/2}$	$g^2_{7/2}d^2_{5/2}d^0_{3/2}$	$9/2^-_1$	30%	$p^1_{1/2}g^6_{9/2}$	$g^2_{7/2}d^2_{5/2}d^0_{3/2}$
$17/2^+_1$	27%	$p^2_{1/2}g^5_{9/2}$	$g^2_{7/2}d^2_{5/2}d^0_{3/2}$	$13/2^-_1$	32%	$p^1_{1/2}g^6_{9/2}$	$g^2_{7/2}d^2_{5/2}d^0_{3/2}$
$15/2^+_1$	21%	$p^2_{1/2}g^5_{9/2}$	$g^2_{7/2}d^2_{5/2}d^0_{3/2}$	$11/2^-_1$	18%	$p^1_{1/2}g^6_{9/2}$	$g^1_{7/2}d^3_{5/2}d^0_{3/2}$
$19/2^+_1$	44%	$p^2_{1/2}g^5_{9/2}$	$g^1_{7/2}d^3_{5/2}d^0_{3/2}$	$13/2^-_2$	20%	$p^1_{1/2}g^6_{9/2}$	$g^1_{7/2}d^3_{5/2}d^0_{3/2}$
$21/2^+_1$	29%	$p^2_{1/2}g^5_{9/2}$	$g^2_{7/2}d^2_{5/2}d^0_{3/2}$	$17/2^-_1$	37%	$p^1_{1/2}g^6_{9/2}$	$g^2_{7/2}d^2_{5/2}d^0_{3/2}$
$21/2^+_2$	31%	$p^2_{1/2}g^5_{9/2}$	$g^1_{7/2}d^3_{5/2}d^0_{3/2}$	$15/2^-_1$	25%	$p^1_{1/2}g^6_{9/2}$	$g^2_{7/2}d^2_{5/2}d^0_{3/2}$
$23/2^+_1$	50%	$p^2_{1/2}g^5_{9/2}$	$g^1_{7/2}d^3_{5/2}d^0_{3/2}$	$17/2^-_2$	33%	$p^1_{1/2}g^6_{9/2}$	$g^2_{7/2}d^2_{5/2}d^0_{3/2}$
$25/2^+_1$	32%	$p^2_{1/2}g^5_{9/2}$	$g^2_{7/2}d^2_{5/2}d^0_{3/2}$	$17/2^-_3$	23%	$p^1_{1/2}g^6_{9/2}$	$g^1_{7/2}d^3_{5/2}d^0_{3/2}$
$23/2^+_2$	22%	$p^2_{1/2}g^5_{9/2}$	$g^1_{7/2}d^2_{5/2}d^1_{3/2}$	$21/2^-_1$	40%	$p^1_{1/2}g^6_{9/2}$	$g^2_{7/2}d^2_{5/2}d^0_{3/2}$
$25/2^+_2$	36%	$p^2_{1/2}g^5_{9/2}$	$g^1_{7/2}d^3_{5/2}d^0_{3/2}$	$19/2^-_1$	17%	$p^1_{1/2}g^6_{9/2}$	$g^2_{7/2}d^2_{5/2}d^0_{3/2}$
$27/2^+_1$	56%	$p^2_{1/2}g^5_{9/2}$	$g^1_{7/2}d^3_{5/2}d^0_{3/2}$	$21/2^-_2$	29%	$p^1_{1/2}g^6_{9/2}$	$g^2_{7/2}d^2_{5/2}d^0_{3/2}$
$25/2^+_3$	31%	$p^2_{1/2}g^5_{9/2}$	$g^1_{7/2}d^3_{5/2}d^0_{3/2}$	$23/2^-_1$	22%	$p^1_{1/2}g^6_{9/2}$	$g^2_{7/2}d^2_{5/2}d^0_{3/2}$
$29/2^+_1$	33%	$p^2_{1/2}g^5_{9/2}$	$g^2_{7/2}d^2_{5/2}d^0_{3/2}$	$25/2^-_1$	40%	$p^1_{1/2}g^6_{9/2}$	$g^2_{7/2}d^2_{5/2}d^0_{3/2}$
$27/2^+_2$	24%	$p^2_{1/2}g^5_{9/2}$	$g^1_{7/2}d^2_{5/2}d^1_{3/2}$	$25/2^-_2$	47%	$p^1_{1/2}g^6_{9/2}$	$g^1_{7/2}d^3_{5/2}d^0_{3/2}$
$29/2^+_2$	35%	$p^2_{1/2}g^5_{9/2}$	$g^1_{7/2}d^3_{5/2}d^0_{3/2}$	$27/2^-_1$	26%	$p^1_{1/2}g^6_{9/2}$	$g^1_{7/2}d^3_{5/2}d^0_{3/2}$
$27/2^+_3$	33%	$p^2_{1/2}g^5_{9/2}$	$g^2_{7/2}d^2_{5/2}d^0_{3/2}$	$29/2^-_1$	45%	$p^1_{1/2}g^6_{9/2}$	$g^2_{7/2}d^2_{5/2}d^0_{3/2}$
$29/2^+_3$	24%	$p^2_{1/2}g^5_{9/2}$	$g^1_{7/2}d^3_{5/2}d^0_{3/2}$	$31/2^-_1$	43%	$p^1_{1/2}g^6_{9/2}$	$g^1_{7/2}d^3_{5/2}d^0_{3/2}$
$31/2^+_1$	59%	$p^2_{1/2}g^5_{9/2}$	$g^1_{7/2}d^3_{5/2}d^0_{3/2}$	$33/2^-_1$	53%	$p^1_{1/2}g^6_{9/2}$	$g^2_{7/2}d^2_{5/2}d^0_{3/2}$
$31/2^+_2$	33%	$p^2_{1/2}g^5_{9/2}$	$g^1_{7/2}d^2_{5/2}d^1_{3/2}$	$37/2^-_1$	54%	$p^1_{1/2}g^6_{9/2}$	$g^2_{7/2}d^2_{5/2}d^0_{3/2}$
$33/2^+_1$	32%	$p^2_{1/2}g^5_{9/2}$	$g^1_{7/2}d^3_{5/2}d^0_{3/2}$	$39/2^-_1$	77%	$p^1_{1/2}g^6_{9/2}$	$g^2_{7/2}d^2_{5/2}d^0_{3/2}$
$31/2^+_3$	55%	$p^2_{1/2}g^5_{9/2}$	$g^1_{7/2}d^3_{5/2}d^0_{3/2}$				

while it is observed 137 keV below the $7/2^+$ state. The lowest observed positive-parity state is $9/2^+$ and corresponds to wave function consisting of the $\pi(p^2_{1/2}g^5_{9/2}) \otimes \nu(g^2_{7/2}d^2_{5/2})$ configuration with an amplitude of 30%.

The first excited $7/2^+$, $9/2^+$, $11/2^+$, $13/2^+$, $15/2^+$, $17/2^+$, $21/2^+$, $25/2^+$ and $29/2^+$ observed states are explained with $\pi(p^2_{1/2}g^5_{9/2}) \otimes \nu(g^2_{7/2}d^2_{5/2})$ configuration. The first excited $19/2^+$, $23/2^+$, $27/2^+$ and $31/2^+$, and the second excited $21/2^+$, $25/2^+$ and $29/2^+$ observed states are obtained by $\pi(p^2_{1/2}g^5_{9/2}) \otimes \nu(g^1_{7/2}d^3_{5/2}d^0_{3/2})$ configuration, *i.e.*, excitation of $\nu g_{7/2}$ to $\nu d_{5/2}$ orbital. The second excited $23/2^+$, $27/2^+$ and $31/2^+$ predicted states have reasonable good agreement with the experimental results and are obtained by $\pi(p^2_{1/2}g^5_{9/2}) \otimes \nu(g^1_{7/2}d^2_{5/2}d^1_{3/2})$ configuration, *i.e.*, by excitation of a $\nu g_{7/2}$ to $\nu d_{3/2}$ orbital. The first excited $35/2^+$ state is also predicted to be based on the same configuration and exhibit agreement with the observed state at 7083 keV. The first excited $35/2^+$ state predicted to be based on $\pi(p^2_{1/2}g^5_{9/2}) \otimes \nu(g^1_{7/2}d^3_{5/2}d^0_{3/2})$ configuration shows noticeable disagreement. Higher spin states also exhibit significant deviations.

In general, the ordering of levels have been reproduced very well by the shell-model calculations. In fact, calculations overestimate the experimentally observed levels, which is possibly due to limited model space used for neutrons.

The negative-parity states in band B4 have been included in Fig. 2 for comparison as the $h_{11/2}$ neutrons have not been included in the present calculations. The details of wave functions for the negative-parity states of ^{99}Rh are also given in Table I. The ground state $1/2^-$ is well-predicted by $jj45pna$ interaction and the wave function consists of $\pi(p^1_{1/2}g^6_{9/2}) \otimes \nu(g^2_{7/2}d^2_{5/2})$ configuration with an amplitude of 35%. It is observed that the first excited $5/2^-$ state lies at 427 keV above the $1/2^-$ ground state, whereas the calculated excitation energy is 288 keV. The $9/2^-$ and $13/2^-$ states are predicted at 705 and 1279 keV by calculations which are underestimated compared to the experimental 979 and 1660 keV values, respectively. In calculations, the dominant contribution from the $\pi(p^1_{1/2}g^6_{9/2}) \otimes \nu(g^2_{7/2}d^2_{5/2})$ configuration has been observed up to $37/2^-$ state. The ordering of levels has been reproduced well by the shell-model calculations. Theoretically obtained excitation energies are underpredicted as compared to the experimental data. It requires to re-tune the two-body matrix elements or readjust the single-particle energies in this interaction.

Singh *et al.* [17] have performed shell-model calculations for ^{99}Rh using the code OXBASH [18] with the model space encompassing the $\pi(p_{1/2}g_{9/2})$ and $\nu(d_{5/2}s_{1/2})$ orbitals outside the ^{88}Sr core. The level structures up to moderate spins $31/2^+$ and $21/2^-$ are well-reproduced thus can be thought to exhibit single-particle behavior. The $\nu(g_{7/2}h_{11/2})$ orbitals were not included in the calculations which are expected to include the higher angular momentum states. The present calculations using $jj45pna$ interaction exhibit better agreement for the low-lying negative-parity states compared to Gloeckner interaction used by Singh *et al.* [17]. The present calculations performed with comparatively larger model space, significantly improve the predictive power of calculations and the level energies are in good agreement with experimental ones up to higher spin states.

3. Systematics of bands observed in odd-*A* Rh isotopes

Systematics of the observed $\pi p_{1/2}$ and $\pi g_{9/2}$ bands in the odd-A $^{91-113}$Rh isotopes ($N = 46$–68) are shown in Figs. 3 and 4, respectively. It is evident from these figures that the $1/2^-$ level from the $\pi p_{1/2}$ orbital forms the ground state in the odd-A $^{99-103}$Rh isotopes, whereas the $9/2^+$ and $7/2^+$ states from the $\pi g_{9/2}$ orbital form the ground state in the lighter $^{91-97}$Rh isotopes and the heavier $^{105-113}$Rh isotopes, respectively. Moreover, the $9/2^+$ state becomes the quasi-ground state in ^{99,101}Rh, *i.e.*, it lies lower in energy than the $7/2^+$ state and above the $1/2^-$ ground state. Similarly, the $7/2^+$ state becomes the quasi-ground state in ^{103}Rh, *i.e.*, it lies lower in energy than the $9/2^+$ state and above the $1/2^-$ ground state. The energy differences between the $7/2^+$ and $9/2^+$ states from the $\pi g_{9/2}$ orbital in the odd-A $^{99-113}$Rh [2, 8, 19–21] isotopes are +65, +25, −93, −149, −194, −206, −211 and −212 keV, respectively, which exhibit a smooth change in sign at ^{103}Rh ($N = 58$). In the case of nuclei with odd nucleon in the orbit with angular momentum j, the states with spin j and spin $j-1$ have been generally observed to compete [22]. Bohr and Mottleson [23] have pointed out that the appearance of the spin $(j-1)$ state as the ground state in the case of odd-Z isotopes is possibly related to the onset of quadrupole deformation in isotopes due to the rearrangement of proton orbitals as a function of neutron number.

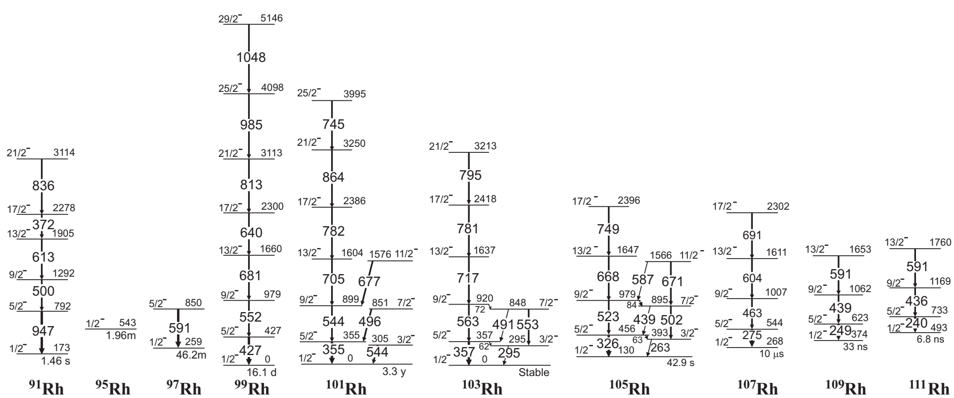

Fig. 3. Systematics of excited states in the single-quasiparticle $\pi p_{1/2}$ bands observed in the odd-A $^{91-113}$Rh isotopes [2, 8, 19–21, 24–27].

The $13/2^+ \to 9/2^+$ transition energies in the $\pi g_{9/2}$ bands in the case of the odd-A $^{91-101}$Rh isotopes show near constancy. The ^{95}Rh isotope (with $N = 50$ neutron shell closure) is exception where a sharp jump in the energy is observed. The onset of deformation is noticeable at $N = 60$, which is indicated by beginning of regular decrease in the $13/2^+ \to 9/2^+$

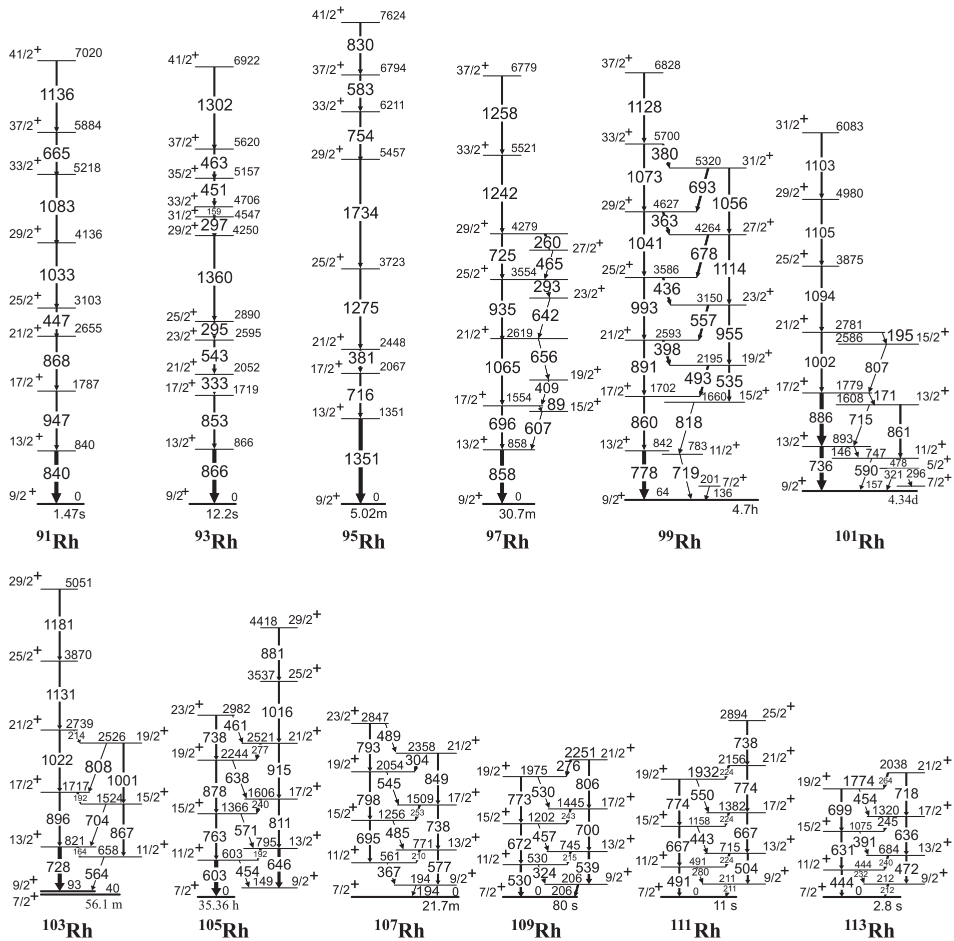

Fig. 4. Systematics of excited states in the single-quasiparticle $\pi g_{9/2}$ bands observed in the odd-A $^{91-113}$Rh isotopes [2, 8, 19–21, 24–27].

transition energy with increase in neutron number (Fig. 4). The increase in deformation continues for the heavier odd-A $^{103-113}$Rh isotopes. Similar variation in the relative position of the $5/2^+$, $7/2^+$ and $9/2^+$ states has been observed in the $^{97-105}$Tc isotopes, where regular order of these states occurs for ^{103}Tc ($N = 60$) and heavier isotopes [28]. The shape transition which occurs as neutrons are added beyond $N = 58$ has also been noticed in even–even nuclei around $Z = 40$ [28]. Both the signature partners are observed in the $\pi g_{9/2}$ band for the odd-A $^{97-113}$Rh isotopes, whereas for the lighter odd-A $^{91-95}$Rh isotopes, only the favored signature partner is observed. The plot of the staggering parameter, $[E(I) - E(I-1)]/2I$, *vs.* spin for the odd-A $^{99-113}$Rh isotopes is shown in Fig. 5. It shows decrease in staggering with increasing neutron number and hence can be related with increase in deformation in these isotopes. The observed $\pi p_{1/2}$ band in the odd-A $^{91-111}$Rh isotopes is decoupled one with the rotational band transition energies showing a regular decrease with increase in neutron number.

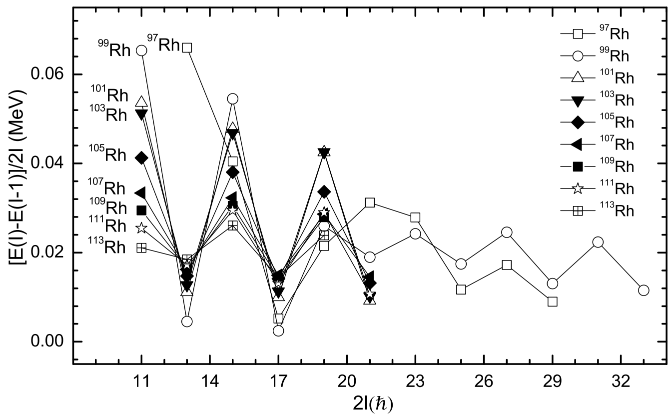

Fig. 5. Energy staggering, $[E(I)–E(I-1)]/2I$, parameter plotted as a function of spin for the $\pi g_{9/2}$ bands in the odd-A $^{99-113}$Rh isotopes [2, 8, 19–21].

The energies of the γ transitions in the $\pi p_{1/2}$ and $\pi g_{9/2}$ bands in the odd-A $^{91-113}$Rh [2, 8, 19–21, 24–27] isotopes along with those in the ground state bands in the corresponding core $^{90-112}$Ru [29–39] isotopes are plotted in Fig. 6 as a function of spin. Systematic comparison of the single-quasiparticle $\pi p_{1/2}$ and $\pi g_{9/2}$ bands in Rh isotopes and the ground state bands in the respective even–even core Ru isotopes is shown in Fig. 6. It infers ability of the odd hole or particle to polarize the γ-soft core to a stable deformation. The energies of the $5/2^- \to 1/2^-$ gamma transitions in the $\pi p_{1/2}$ bands, and the $13/2^+ \to 9/2^+$ gamma transitions in the $\pi g_{9/2}$ bands in the odd-A $^{91-113}$Rh isotopes have been plotted in Fig. 7 as a function of spin along with the corresponding $2^+ \to 0^+$ gamma-transition in the ground state band of the respective even–even core $^{90-112}$Ru isotones [29–39]. Such a comparison should be valid for the spherical nuclei in the weak-coupling limit and also for the deformed nuclei when the Fermi surface lies near low-K orbits, *i.e.*, decoupled bands. The odd-A nuclei under consideration are transitional, and none of them is strongly deformed.

The excitation energy ratios $(E_{4^+} \to E_{0^+})/(E_{2^+} \to E_{0^+})$ for the even–even $^{90-112}$Ru isotopes are plotted and shown in Fig. 7. The corresponding excitation energy ratios: $(E_{17/2^+} \to E_{9/2^+})/(E_{13/2^+} \to E_{9/2^+})$, for the $\pi g_{9/2}$ bands and $(E_{9/2^-} \to E_{1/2^-})/(E_{5/2^-} \to E_{1/2^-})$ for the $\pi p_{1/2}$ bands in odd-A Rh isotopes are also included in Fig. 7. In the odd-A $^{103-113}$Rh ($N = 58$–68) isotopes, where $7/2^+$ is the ground state, the excitation energy ratios,

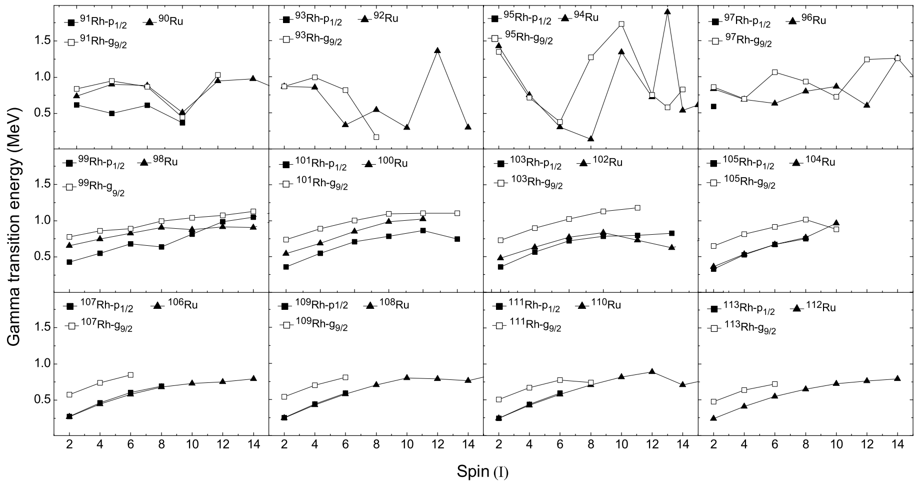

Fig. 6. The energies of the γ transitions in the $\pi p_{1/2}$ and $\pi g_{9/2}$ bands in the odd-A $^{91-113}$Rh isotopes [2, 8, 19–21, 24–27] along with those in the ground state bands in the corresponding the $^{90-112}$Ru core isotopes [29–39] plotted as a function of spin. The $5/2^- \to 1/2^-$ transition in the $\pi p_{1/2}$ band and the $13/2^+ \to 9/2^+$ transition in the $\pi g_{9/2}$ band in odd-A Rh isotopes have been plotted corresponding to the $2^+ \to 0^+$ transition in the ground state band in the even–even $^{90-112}$Ru core isotopes. There are no data points corresponding to the $\pi p_{1/2}$ band in the ^{93,95,113}Rh isotopes.

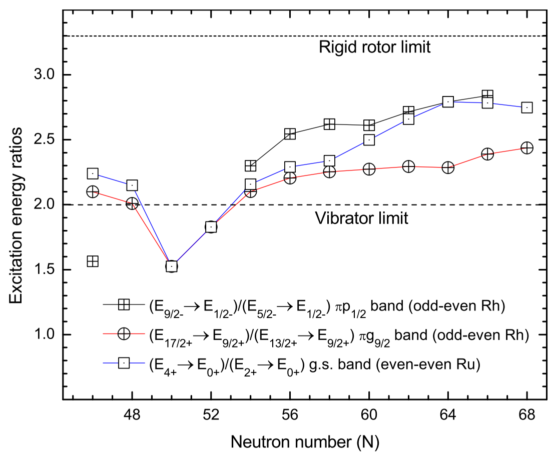

Fig. 7. The comparison of the excitation energy ratios, $(E_{17/2^+} \to E_{9/2^+})/(E_{13/2^+} \to E_{9/2^+})$, for the $\pi g_{9/2}$ bands and $(E_{9/2^-} \to E_{1/2^-})/(E_{5/2^-} \to E_{1/2^-})$ for the $\pi p_{1/2}$ bands for the odd-A $^{91-113}$Rh [2, 8, 19–21, 24–27] isotopes with the excitation energy ratios $(E_{4^+} \to E_{0^+})/(E_{2^+} \to E_{0^+})$ for the even–even $^{90-112}$Ru [29–39] isotopes.

$(E_{15/2^+} \to E_{7/2^+})/(E_{11/2^+} \to E_{7/2^+})$, for the $\pi g_{9/2}$ bands have closely the same values as for the $(E_{17/2^+} \to E_{9/2^+})/(E_{13/2^+} \to E_{9/2^+})$ ratios. The excitation energy ratios for the $\pi g_{9/2}$ bands for the odd-A $^{91-103}$Rh ($N =$ 46–58) isotopes closely follow the corresponding values for the even–even $^{90-102}$Ru ($N = 46$–58) core isotopes (Fig. 7). The γ-transition energy plots for the even–even Ru core finally merge with the $\pi p_{1/2}$ band for the heavier $^{105-111}$Rh isotopes [2, 20, 21]. The ^{90,92}Ru [32, 33] and $^{98-102}$Ru [29, 30, 34] isotopes are vibrational, and the heavier $^{104-112}$Ru isotopes [35–39] are quasi-rotational (Fig. 7).

As is evident from Fig. 7, the excitation energy ratio values for the $\pi p_{1/2}$ band are larger than the $\pi g_{9/2}$ band for the odd-A $^{99-111}$Rh isotopes [2, 8, 19–21], which indicates more rotational character for the $\pi p_{1/2}$ band. It is likely to be the effect of deformation induced by the $\pi\nu$ interaction between SOP orbitals. The number of protons in the $g_{9/2}$ orbitals is larger in the case of the $\pi p_{1/2}$ band when a single proton occupies the $p_{1/2}$ orbital as compared to the case of the $\pi g_{9/2}$ band when two particles occupy the $p_{1/2}$ orbital. In the case of the $\pi p_{1/2}$ band, the larger number of protons in the $g_{9/2}$ orbital lowers the energies of the $g_{7/2}$ and the $h_{11/2}$ neutron orbitals, so it becomes energetically favorable to raise neutrons to these orbitals. The increase in occupation probability of $g_{7/2}$ and $h_{11/2}$ neutron orbitals, in turn, increases the $\pi\nu$ interaction strength for the $\pi p_{1/2}$ configuration, which effectively cancels out the spherically driven $\nu\nu$ and $\pi\pi$ pairing correlations [40]. It infers the importance of the spin–orbit partner orbitals for deformation in this region.

An interesting feature of the observed spectra is that unusual shape transition appearing in the lighter even–even $^{90-96}$Ru ($N = 46$–52) core is also closely reflected in the plots for the $\pi g_{9/2}$ bands in the respective odd-mass Rh nuclei. The excitation energy of the 2^+ state in the ^{90,92}Ru ($N = 46$, 48) isotopes [31, 33] is ~ 0.75 MeV and shows a sudden sharp jump to 1.43 MeV for the ^{94}Ru isotope, and recovers to ~ 0.75 MeV for the ^{96}Ru isotope. Further, 2^+ state excitation energy shows regular and significant decrease to ~ 0.27 MeV till ^{104}Ru is reached and it remains almost constant for the heavier even–even $^{106-112}$Ru isotopes [36–39]. The systematics of the low-lying states in the even–even $^{90-112}$Ru isotopes have been intricately linked with the nature of $\pi\nu$ interaction operating between SOP orbitals — the $(\pi d_{5/2}, \nu d_{3/2})$ and $(\pi g_{9/2}, \nu g_{7/2})$ orbitals, which cause collectivity in nuclei [41].

4. Conclusions

The level scheme of the transitional nucleus ^{99}Rh has been studied within the framework of shell-model calculations. The present calculations are done by using $jj45pna$ interaction, which are in better agreement experimentally.

The observed structures at low and medium spins are compared with the shell-model calculations in the ($p_{1/2}$, $g_{9/2}$) proton space and the ($g_{7/2}$, $d_{5/2}$, $d_{3/2}$, $s_{1/2}$) neutron space. The systematics of the single-quasiparticle $\pi g_{9/2}$ and $\pi p_{1/2}$ bands in odd-A Rh isotopes are discussed.

Authors acknowledge the joint effort of IUAC, New Delhi, TIFR, Mumbai, UGC-DAE CSR and SINP, Kolkata, for establishing the INGA clover array. Financial support from UGC, and IUAC (project No. IUAC/XIII.7/UFR-54315) New Delhi, under the Center of Advanced Study Funds, FIST, is duly acknowledged.

REFERENCES

[1] A.D. Ayangeakaa *et al.*, *Phys. Rev. Lett.* **110**, 102501 (2013).
[2] J.A. Alcántara-Núñez *et al.*, *Phys. Rev. C* **69**, 024317 (2004).
[3] B. Cederwall *et al.*, *Nature* **469**, 68 (2011).
[4] J. Gizon *et al.*, *Phys. Lett. B* **410**, 95 (1997).
[5] C. Vaman *et al.*, *Phys. Rev. Lett.* **92**, 032501 (2004).
[6] P. Joshi *et al.*, *Phys. Lett. B* **595**, 135 (2004).
[7] J. Timár *et al.*, *Phys. Rev. C* **73**, 011301(R) (2006).
[8] J. Timár *et al.*, *Nucl. Phys. A* **696**, 241 (2001).
[9] R.F. Casten, D.D. Warner, D.S. Brenner, R.L. Gill, *Phys. Rev. Lett.* **47**, 1433 (1981).
[10] S. Kumar *et al.*, *J. Phys. G: Nucl. Part. Phys.* **41**, 105110 (2014).
[11] M. Czerwiński *et al.*, *Phys. Rev. C* **92**, 014328 (2015).
[12] T. Materna *et al.*, *Phys. Rev. C* **92**, 034305 (2015).
[13] Z.Q. Li *et al.*, *Phys. Rev. C* **94**, 014315 (2016).
[14] E. Browne, J.K. Tuli, *Nucl. Data Sheets* **112**, 275 (2011).
[15] B.A. Brown, W.D.M. Rae, NuShell@MSU, MSU-NSCL report, 2007.
[16] M. Hjorth-Jensen, T. Kuo, E. Osnes, *Phys. Rep.* **261**, 125 (1995).
[17] R.P. Singh, R.K. Bhowmik, S.S. Ghugre, S.B. Patel, *Eur. Phys. J. A* **7**, 35 (2000).
[18] B.A. Brown, A. Etchegoyen, W.D.M. Rae, N.S. Godwin, MSU-NSCL report number 524, 1985 (unpublished).
[19] H. Dejbakhsh, R.P. Schmitt, G. Mouchaty, *Phys. Rev. C* **37**, 621 (1988).
[20] Ts. Venkova *et al.*, *Eur. Phys. J. A* **6**, 405 (1999).
[21] Ts. Venkova *et al.*, *Eur. Phys. J. A* **15**, 429 (2002).
[22] A. Kuriyama, T. Marumori, K. Matsugamagi, *Prog. Theor. Phys. Suppl.* **58**, 53 (1975).

[23] A. Bohr, B. Mottelson, *Mat. Fys. Medd. Dan. Vid. Selsk.* **27**, 16 (1953).

[24] N. Mărginean *et al.*, *Phys. Rev. C* **72**, 014302 (2005).

[25] H.A. Roth *et al.*, *J. Phys. G: Nucl. Part. Phys.* **21**, L1 (1995).

[26] H.A. Roth *et al.*, *Phys. Rev. C* **50**, 1330 (1994).

[27] W.F. Piel, G. Scharff-Goldhaber, C.J. Lister, B.J. Varley, *Phys. Rev. C* **33**, 512 (1986).

[28] A. Bauchet *et al.*, *Eur. Phys. J. A* **10**, 145 (2001).

[29] J. Timár *et al.*, *Phys. Rev. C* **62**, 044317 (2000).

[30] B. Kharraja *et al.*, *Phys. Rev. C* **57**, 83 (1998).

[31] D. Bucurescu *et al.*, *Phys. Rev. C* **69**, 064319 (2004).

[32] C. Lingk *et al.*, *Phys. Rev. C* **56**, R2349 (1997).

[33] A. Jungclaus *et al.*, *Phys. Rev. C* **60**, 014309 (1999).

[34] D. Sohler *et al.*, *Phys. Rev. C* **71**, 064302 (2005).

[35] J. Srebrny *et al.*, *Nucl. Phys. A* **766**, 25 (2006).

[36] M. Sanchez-Vega *et al.*, *Eur. Phys. J. A* **35**, 159 (2008).

[37] Che Xing-Lai *et al.*, *Chin. Phys. Lett.* **21**, 1904 (2004).

[38] Jiang Zhuo *et al.*, *Chin. Phys. Lett.* **20**, 350 (2003).

[39] Che Xing-Lai *et al.*, *Chin. Phys. Lett.* **23**, 328 (2006).

[40] H. Dejbakhsh, *Phys. Lett. B* **210**, 50 (1988).

[41] Arun Bharti, S.K. Khosa, *Nucl. Phys. A* **572**, 317 (1994).